

SCIENTIFIC REPORTS



OPEN

Publisher Correction: Alpha-synuclein facilitates to form short unconventional microtubules that have a unique function in the axonal transport

Shiori Toba¹, Mingyue Jin¹, Masami Yamada¹, Kanako Kumamoto¹, Sakiko Matsumoto¹, Takuo Yasunaga^{2,3,4}, Yuko Fukunaga^{5,6}, Atsuo Miyazawa^{5,6}, Sakiko Fujita⁷, Kyoko Itoh⁸, Shinji Fushiki⁸, Hiroaki Kojima⁹, Hideki Wanibuchi¹⁰, Yoshiyuki Arai¹¹, Takeharu Nagai¹¹ & Shinji Hirotsune¹

Correction to: *Scientific Reports* <https://doi.org/10.1038/s41598-017-15575-3>, published online 27 November 2017

In this Article, Figure 5 was inadvertently published as Figures 5 and 6, leading to the incorrect publication of Figure 6 as Figure 7 and the omission of the correct Figure 7. The correct Figures 5, 6, and 7 appear below as Figures 1, 2, and 3 respectively. The Figure legends are correct.

¹Department of Genetic Disease Research, Osaka City University Graduate School of Medicine, Asahi-machi 1-4-3 Abeno, Osaka, 545-8585, Japan. ²Department of Bioscience and Bioinformatics, Faculty of Computer Science and Systems Engineering, Kyushu Institute of Technology, Kawazu 680-4, Iizuka, Fukuoka, 820-850, Japan. ³JST-SENTAN, 4-1-8, Honcho, Kawaguchi, Saitama, 332-0012, Japan. ⁴JST-CREST, 4-1-8, Honcho, Kawaguchi, Saitama, 332-0012, Japan. ⁵Graduate School of Life Science, University of Hyogo, 3-2-1 Kouto, Kamigori-cho, Ako-gun, Hyogo, 678-1297, Japan. ⁶RSC-University of Hyogo Leading Program Center, RIKEN SPring-8 Center, 1-1-1 Kouto, Sayo-cho, Sayo-gun, Hyogo, 679-5148, Japan. ⁷Graduate School of Materials Science, Nara Institute of Science and Technology, 8916-5, Takayama, Ikoma, Nara, 630-0101, Japan. ⁸Department of Pathology and Applied Neurobiology, Kyoto Prefectural University of Medicine Graduate School of Medical Sciences, Kajji-cho, Kawaramachi-Hirokoji, Kamigyo-ku, Kyoto, 602-8566, Japan. ⁹Advanced ICT Research Institute, National Institute of Information and Communications Technology, 588-2 Iwaoka, Nishi-ku, Kobe, 651-2492, Japan. ¹⁰Department of Pathology, Osaka City University Graduate School of Medicine, Asahi-machi 1-4-3 Abeno, Osaka, 545-8586, Japan. ¹¹Department of Biomolecular Science and Engineering, Institute of Scientific and Industrial Research, Osaka University, Mihoga-oka 8-1, Osaka, 567-0047, Japan. Shiori Toba and Mingyue Jin contributed equally to this work. Correspondence and requests for materials should be addressed to S.H. (email: shinjih@med.osaka-cu.ac.jp)

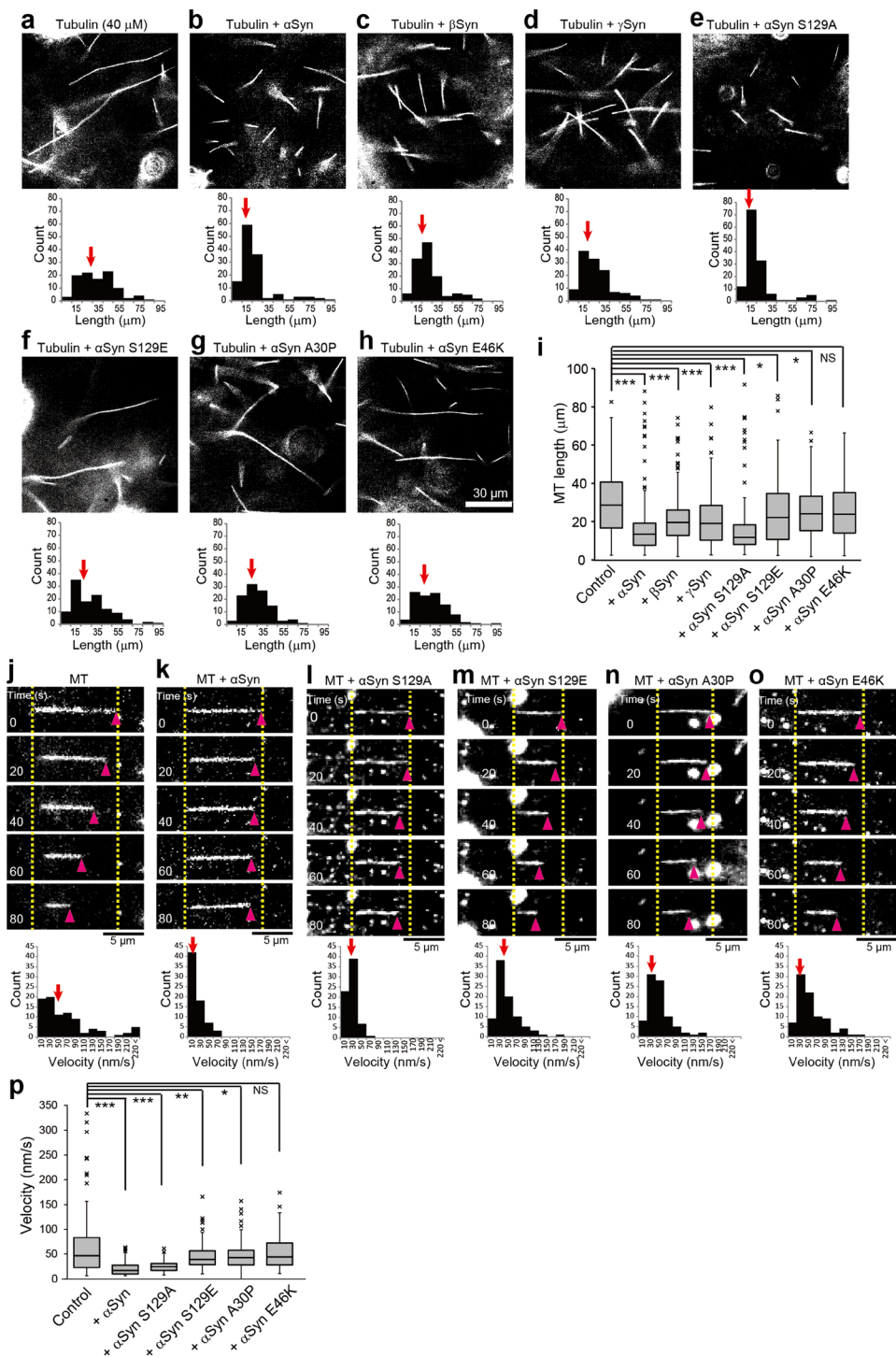


Figure 1. Effect of Syn on tubulin polymerization and depolymerization. **(a–h)** MTs undergoing polymerization with unlabeled tubulin in vitro were visualized using dark-field light microscopy. Tubulin polymerization was performed without Syn **(a)** and with αSyn **(b)**, βSyn **(c)**, γSyn **(d)**, $\alpha\text{Syn S129A}$ **(e)**, $\alpha\text{Syn S129E}$ **(f)**, $\alpha\text{Syn A30P}$ **(g)**, or $\alpha\text{Syn E46K}$ **(h)**. MT length with or without Syn was measured and is shown beneath each image. The median values are indicated by red arrows. Scale bar: 30 μm . **(i)** Box-and-whisker plots of the lengths of MTs polymerized in vitro ($N = 100$ for each condition). **(j–o)** Effect of αSyn s on MT stabilization. Unilaterally occurring spontaneous depolymerization was measured in vitro without αSyn s **(j)** and with αSyn **(k)**, $\alpha\text{Syn S129A}$ **(l)**, $\alpha\text{Syn S129E}$ **(m)**, $\alpha\text{Syn A30P}$ **(n)**, or $\alpha\text{Syn E46K}$ **(o)**. The distributions of the depolymerization velocities are shown beneath each image set. Spontaneous depolymerization proceeded unilaterally in each case. The pink arrowheads indicate the tips of depolymerizing MTs, and the dotted yellow lines indicate the original lengths of the MTs. The median values are indicated by red arrows. Scale bar: 5 μm . **(p)** Box-and-whisker plots of the spontaneous depolymerization velocities ($N = 80$ in each condition). P values in **(i)** and **(p)** were calculated with t-test of nonparametric test, mean \pm SEM; *** $p < 0.001$, ** $p < 0.01$, * $p < 0.05$, “NS” means not significant. See also Supplementary Videos 6 and 7.

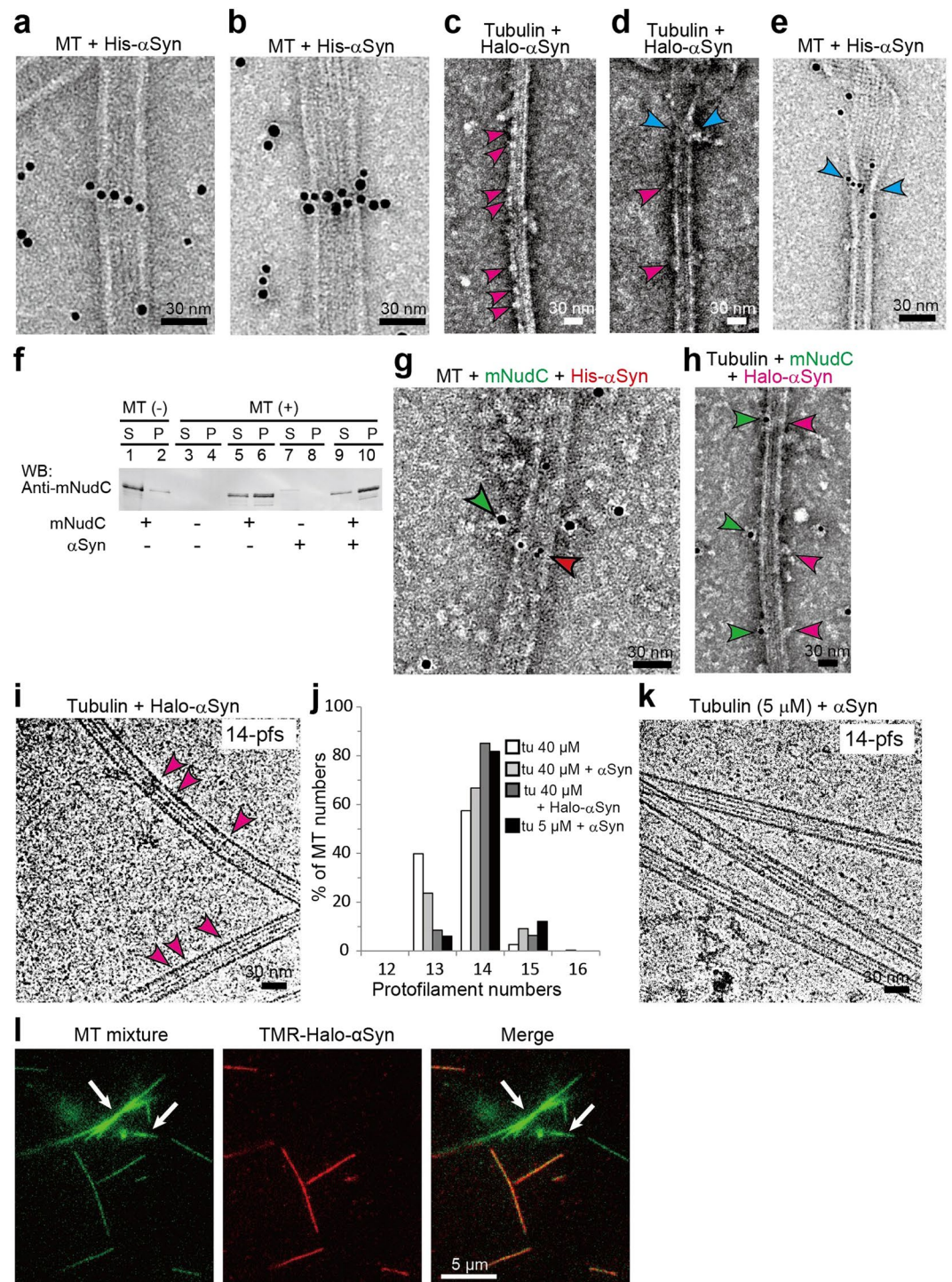


Figure 2. Characterization of α Syn binding to MTs using colloidal gold particles and Halo-tags. (a,b) α Syn binding to MTs was analyzed by transmission electron microscope (TEM). MTs were mixed with colloidal gold-labeled α Syn (Gold- α Syn) and negatively stained with 2% of uranyl acetate. Gold- α Syn was prepared from N-terminal His-tagged α Syn (His- α Syn). Gold- α Syns appeared as string-like α Syn polymers on MTs. (c) TEM image of MT polymerized with Halo-tagged α Syn (Halo- α Syn). Bamboo joint-like structures (indicated by magenta arrowheads) are visible on the MTs. (d) MT end structure with Halo- α Syn. Joint-like structures similar to those shown in (c) are indicated by magenta arrowheads. Halo- α Syns were also observed in the zone between the outwardly opened tubulin sheet and MT cylinder (blue arrowheads). (e) Gold- α Syn located at the transition zone (blue arrowheads). (f) MT pull-down assay. mNudC co-precipitated with MTs was examined in the absence and presence of α Syn. (g) Dual labeling immunoelectron microscopy (IEM) used to visualize the interaction of MT with mNudC and α Syn. mNudC was labeled with 10 nm colloidal gold (green) via anti-mNudC antibody; and His- α Syn was labeled with 5 nm colloidal gold (red). Co-localization of mNudC and α Syn on a MT is indicated by arrowheads. (h) MT polymerized with Halo- α Syn (magenta) and Gold-mNudC (green). Bamboo joint-like structures (magenta) and colloidal gold (green) indicate co-localization

of mNudC with Halo- α Syn on a MT. **(i)** Cryo-TEM image of MTs polymerized with Halo- α Syn. Joint-like structures on MTs are indicated by magenta arrowheads. MT pfs numbers determined from Moiré patterns are indicated at the top right. **(j)** Distribution of the pfs numbers of polymerized MTs. The MTs assembled from 40 μ M of tubulin (tu) without paclitaxel stabilization mainly formed 13- and 14-pfs MTs (for tu 40 μ M, N = 261). The addition of α Syn clearly increased the number of MTs carrying 14-pfs even at 5 μ M tubulin (tu 40 μ M + α Syn, N = 259; tu 40 μ M + Halo- α Syn, N = 135; tu 5 μ M + α Syn, N = 111). **(k)** Cryo-TEM image of MTs polymerized with α Syn and 5 μ M of tubulin. MT pfs numbers determined from Moiré patterns are indicated at the top right. Bar: 30 nm. **(l)** Selective binding of α Syn to MTs. A mixture of axoneme-nucleated MTs (axoneme-MTs) and GMPCPP polymerized MTs (GMPCPP-MTs) was incubated with TMR-Halo- α Syn (red) in a chamber. The white arrows indicate axoneme-MTs; narrow MTs correspond to GMPCPP-MTs. TMR-Halo- α Syn appears to preferentially bind to GMPCPP-MTs, but not to axoneme-MTs. Scale bar: 30 nm in **(a–e)**, **(g–i)** and **(k)**; and 5 μ m in **(l)**.

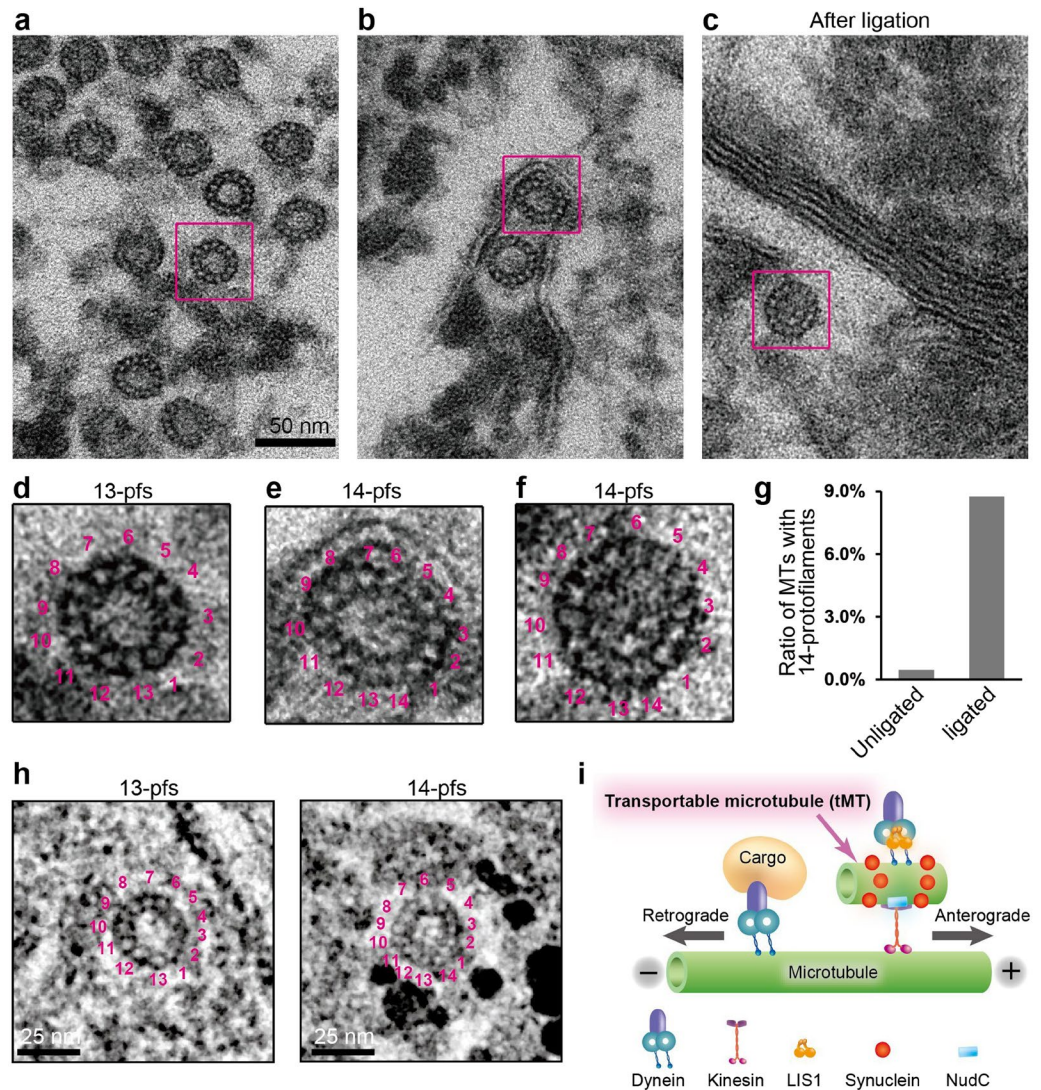


Figure 3. Unconventional MTs carrying 14-pfs in rat femoral nerves. Rat femoral nerves with or without ligation were embedded into resin block and examined by TEM. (a) Overview of a micrograph with conventional MTs carrying 13-pfs. The rectangle surrounded area was enlarged and shown in (d). (b) Overview of a micrograph showing unconventional MTs containing 14-pfs. The rectangle surrounded area was enlarged and shown in (e). (c) Overview image of the ligated femoral nerve. Unconventional MTs were captured in ligated nerve, and the rectangle surrounded area was enlarged and shown in (f). (g) Comparison of unconventional MTs in unligated and ligated femoral nerves. The percentage of MTs with 14-pfs in the unligated femoral nerve is 0.5% (10 of 2016 MTs), in the ligated nerve is 8.8% (22 of 230 MTs). (h) Localization of α Syn in femoral nerves visualized by IEM. Silver-enhanced gold particles are observed surrounding fuzzy material around MTs with 14-pfs (right panel), but are not visible in MTs with 13-pfs (left panel). (i) Model for the tMT in the anterograde transport of cytoplasmic dynein by kinesin-1. LIS1 anchors cytoplasmic dynein to a Syn-stabilized tMT followed by the tethering to a kinesin molecule under mNudC mediation. Scale bar: 50 nm in (a–c); and 25 nm in (h).



Open Access This article is licensed under a Creative Commons Attribution 4.0 International License, which permits use, sharing, adaptation, distribution and reproduction in any medium or format, as long as you give appropriate credit to the original author(s) and the source, provide a link to the Creative Commons license, and indicate if changes were made. The images or other third party material in this article are included in the article's Creative Commons license, unless indicated otherwise in a credit line to the material. If material is not included in the article's Creative Commons license and your intended use is not permitted by statutory regulation or exceeds the permitted use, you will need to obtain permission directly from the copyright holder. To view a copy of this license, visit <http://creativecommons.org/licenses/by/4.0/>.

© The Author(s) 2018